Performance Comparison and Analysis of Low Power Hall Thruster Operation on Inert and Molecular Propellants

IEPC-2025-559

Presented at the 39th International Electric Propulsion Conference, Imperial College London, London, United Kingdom
14-19 September 2025

Joseph A. Moskovitz* , William P. Brabston† , Dan Lev‡ , Mitchell L. R. Walker§
Georgia Institute of Technology, Atlanta, GA, 30332, USA

and

Maxim Rubanovich¶, Vladimir Balabanov‖
Asher Space Research Institute, Technion, Haifa, 3200003, Israel

Abstract: A detailed experimental investigation into the performance of a low-power Hall effect thruster (HET), Simplified CAMILA, operating on both atomic (Xe, Kr, Ar) and molecular (CO_2, N_2) propellants is performed. The study measures thrust, specific impulse, and internal efficiencies across a range of discharge voltages (∼75-450 V), input powers (∼75-450 W), and magnetic field strengths (∼118-293 G). Xenon consistently delivers the highest anode efficiency (η_A) performance (η_A = 48.74%, 400 W), followed by krypton (η_A = 33.01%, 450 W), argon (η_A = 22.72%, 450 W), CO_2 (η_A = 11.68%, 450 W), and N_2 (η_A = 7.35%, 400 W). Molecular propellants exhibit significantly lower efficiencies and narrower regions of operational stability, and thus require higher volumetric mass flow rates and magnetic field strengths for stable operation. These observations highlight the engineering challenges of maintaining discharge stability with molecular gases, particularly at lower voltages where mass utilization efficiency sharply declines. Mass and current utilization efficiencies improve with power for all propellants—particularly for molecular ones—though beam efficiency remains relatively constant. A previously developed mass utilization efficiency model accurately predicts experimental results for all propellants within the margin of error, with argon exhibiting the largest deviation. Increasing magnetic field strength initially enhances anode efficiency (requiring ∼1.48x stronger fields for molecular gases versus Xe/Kr), but eventually reduces ion beam current, especially in lighter molecular gases, potentially because of increased ion trajectory divergence due to smaller ion cyclotron radii relative to heavier xenon. These findings underscore the challenges and potential of using molecular propellants in low-power HETs. While inert gases remain superior in performance, molecular propellants can sustain operation under optimized conditions. Further thruster design and operational refinements are needed to improve the viability of molecular propellants for future space missions.

*Undergraduate Student, School of Aerospace Engineering, jmoskovitz3@gatech.edu
†PhD Candidate, School of Aerospace Engineering, wbrabston3@gatech.edu
‡Research Engineer, School of Aerospace Engineering, dan.lev@gatech.edu
§Professor and School Chair, School of Aerospace Engineering, mitchell.walker@ae.gatech.edu
¶Research Engineer, Asher Space Research Institute, aerrumax@technion.ac.il
‖Research Engineer, Asher Space Research Institute, balaban@technion.ac.il

Nomenclature

α	= inverse of the Hall parameter (-)
A_{ch}	= discharge channel area at the exit plane (m^2)
B or $\|B\|$	= magnitude of the magnetic field (G)
B_{ratio}	= ratio of I_{inner} to I_{outer} (-)
γ	= beam divergence efficiency (-)
I_b	= beam current (A)
I_d	= discharge current (A)
I_{inner}	= inner magnetic coil current
I_{outer}	= outer magnetic coil current
I_{sp}	= specific impulse (s)
j_D	= discharge current density = $\frac{I_d}{A_{ch}}$ (A/m^2)
k_b	= Boltzmann constant ($J/^\circ K$)
$k_{iz}(T_e)$	= total ionization rate coefficient averaged over a Maxwellian e^- population with T_e (m^3/s)
λ	= mean free path for ionization (m)
$\bar{L}$	= characteristic length (discharge channel length) (m)
L_{acc}	= acceleration region length (m)
m	= propellant neutral mass (kg)
$\dot{m}_A$	= anode mass flow rate ($sccm$)
$\dot{m}_C$	= cathode mass flow rate ($sccm$)
$\dot{m}_{en}$	= entrained mass flow rate ($sccm$)
n_0	= neutral particle number density (m^{-3})
n_e	= electron number density (m^{-3})
n_i	= ion number density (m^{-3})
η_A	= anode efficiency (-)
η_b	= current utilization efficiency (-)
$\eta_{\dot{m}}$	= mass utilization efficiency (-)
η_V	= voltage utilization efficiency (-)
Ω_{ij}	= species fraction (-)
P	= pressure (Pa)
P_d	= discharge power (W)
Φ	= particle flux ($s^{-1} * m^{-2}$)
q	= elementary charge (C)
T	= thrust (N)
T_C	= corrected thrust (N)
T_e	= electron temperature (eV)
T_i	= ion temperature (eV)
T_n	= neutral gas temperature (eV)
V_{CC}	= cathode coupling voltage (V)
V_{CG}	= cathode-to-ground voltage (V)
V_d	= discharge voltage (V)
v_i	= ion velocity (m/s)
v_n	= neutral thermal velocity (m/s)

I. Introduction

The Hall effect thruster (HET) is a space propulsion technology that has become quite common in the past decade[1] thanks to its high specific impulse (I_{sp}),[2] high reliability,[3] and a high thrust-to-power ratio relative to other types of electric propulsion technologies.[4] HETs have notably been used on NASA's Psyche mission,[5] SpaceX's Starlink v2 mini satellite constellation,[6] and numerous LEO and GEO communications satellites.[2] HETs have traditionally operated at powers > 1 kW, but in recent years the demand for lower power HETs (< 1 kW) has increased significantly, specifically thanks to the growing demand to construct Low-Earth Orbit (LEO) "Megaconstellations" proposed by several companies in the United States, Europe, and China.[6]

Micro-satellites (10-100 kg) are power-limited and have historically used chemical propulsion to execute maneuvers in orbit.[7] Low-power (< 500 W) HETs have the opportunity to enhance the capabilities of these satellites thanks to their high I_{sp} relative to their chemical cousins, which reduces required propellant mass, allowing the payload to be heavier.[7] Despite the benefits that HETs yield, when operated in the < 500 W range, HETs suffer from low efficiency (η_A) and shorter operating lifetimes compared to their higher-power counterparts.[7] The lower efficiency in low-power HETs is due to insufficient ionization and low mass utilization efficiency since the surface-to-volume ratio increases as the thruster is downsized.[8] In order to decrease total power consumption, one either needs to decrease the discharge voltage or discharge current; however, since ion exhaust velocity (and thus specific impulse) is proportional to the square root of discharge voltage ($I_{sp} \propto \sqrt{V_d}$), it is traditionally preferred to instead reduce the discharge current to maintain a reasonable I_{sp} on higher-power HETs (one of the major benefits of using electric propulsion (EP) in the first place).[8] However, in a low-power HET, decreasing I_d to maintain I_{sp} will also decrease η_A; therefore, a balancing act is necessary when tuning low-power HET input parameters in order to maintain satisfactory performance metrics. To lower the discharge current, one needs to decrease the mass flow rate, which in turn decreases the gas density within the chamber cavity, resulting in an increase in the ionization mean free path.[8] This means the propellant is more difficult to ionize and the mass utilization efficiency is lower, thus degrading the overall thruster efficiency.[8] This decreased efficiency combined with the aforementioned already reduced efficiency when using molecular propellants presents severe challenges to the practicality of employing molecular propellants in low-power HETs. Smaller thruster geometries can help maintain reasonable gas densities for lower mass flow rates, but HET-downscaling inherently leads to a higher surface-to-volume ratio and greater plasma-wall losses, decreasing thruster efficiency and lifetime, increasing the channel wall erosion rate, and inducing high thermal loads that reduce the magnetic confinement of the electrons circulating in the Hall current.[8]

The vast majority of HETs run on xenon because it is inert, possesses a high ion mass to ionization energy, and achieves a high density under pressure.[9] Xenon is a trace gas extracted from the Earth's atmosphere, and due to the increasing use of xenon in other industries such as anesthesia, automotive lightning systems, and semiconductor manufacturing, and its already high (and often volatile) cost of procurement, there is an economic incentive in exploring alternative propellants for HETs.[9] Global events like the COVID-19 pandemic and the Russia-Ukraine War are disrupting supply chains, and thus there is a high risk for a xenon shortage.[9] Additionally, a large amount of propellant is consumed in pre-orbit ground testing, further driving up the development costs for HETs running on expensive propellants.[10] Therefore, there is much interest in the use of alternative propellants in lieu of xenon for HETs. Molecular propellants such as N_2 and CO_2 have low boiling points and thus are typically stored as gases, so they do not require input sublimation heat like condensable propellants such as bismuth, iodine, and zinc.[9] Additionally, these molecular propellants are very abundant throughout the solar system,[11] allowing for easier in-situ fuel acquisition and processing on celestial objects other than Earth.

Most of the investigations into HETs running on molecular propellants have been within the scope of Air-Breathing Electric Propulsion (ABEP), and limited studies operating on pure N_2, O_2, or CO_2 exist. Cifali et al. tested a > 1 kW HET on pure N_2 and showed poor efficiency peaking in the range of 22-28% anode efficiency.[11] They found that N_2 ionization efficiency was lower than that of Xe, that it increased with discharge voltage, and was strongly non-linear.[11] Thrust mathematically is expected to vary with the square root of discharge voltage ($T \propto \sqrt{V_d}$), but the observed variation for N_2 was steeper. Cifali et al. suspected that atomic ions were more numerous at higher voltages, which could also be confirmed by the observed higher discharge current with a slightly lower mass flow rate. Additionally, this study exclusively ignited the thruster with xenon and then transitioned to pure N_2 or the N_2/O_2 mixture. The same study also noticed substantial material degradation of the anode and discharge channel when operating the thruster with a

N_2/O_2 mixture. A Busek study led by Hohman operated a 1.5-kW HET on a 95.7% CO_2 2.7% N_2 1.6% Ar mixture meant to simulate the Martian atmosphere.[12] With a mass flow rate of 90 sccm and discharge voltage of just over 250 V, they were able to obtain a thrust-to-power ratio of 26.5 mN/kW.[12] The team achieved a thrust of ∼52 mN with a mass flow rate of 80 sccm and a discharge voltage of 350 V.[12] However, as mentioned, this study operated a HET at significantly higher powers and mass flow rates than the tests we conducted, so the results may not translate well. Finally, the study recorded no evidence of oxidation or soot buildup in the thruster after 10 hours of continuous testing, as CO_2 depositing carbon soot on or oxidizing the channel walls was an initial concern of theirs.[12] A recent study run by Shirasu et al., examining the use of water vapor (H_2O) in a low-power HET (233-358 W) yielded an I_{sp} of 550-860 s and anode efficiency of 5-8%.[13] The study further concluded that the mass utilization efficiency was the most degraded internal efficiency compared to standard xenon operation, as further indicated by a large beam divergence and an increase in low-energy ions.[13] The paper proposes that there are additional power loss mechanisms due to reactions unique to polyatomic (molecular) propellants, as indicated by an evaluation of the ionization cost.[13] The research team further found that increasing the discharge voltage from 200-240 V increased the mass utilization efficiency without degrading power utilization, and they suggest that operating at higher voltages could be more suitable for H_2O HETs.[13] A separate recent study conducted by Munro-O'Brien et al. looked at using other gaseous propellants for low-power HETs (300-400 W), comparing Xe to Kr, Ar, Ne, and N_2, finding the following peak values in Table 1.[14]

Table 1: Measured performance parameters for a variety of propellant types as reported by Munro-O'Brien.[14]

	Xe	Kr	Ar	N_2
T (mN)	12.6	6.9	6.6	5.7
η_A (%)	26.3	15.2	9.6	5.4
I_{sp} (s)	2160	1730	1390	1000

This study found that N_2 operated similarly to Ar, and they were able to eventually ignite the thruster with pure N_2;[14] however, only three N_2 data points were collected in this study due to component failure, and further investigation into low-power HET N_2 operation is in order. A recent publication from Tsuchikawa et al. tested CO_2 on a low-power HET and compared it to Xe, finding the following peak values in Table 2.[10]

Table 2: Measured performance parameters for CO_2 as reported by Tsuchikawa.[10]

	Xe	CO_2
T/P (mN/kW)	38.8	19.9
η_A (%)	23.7	7.11
I_{sp} (s)	1245	727

Thus far, no thorough effort has been made to test the operation of low-power HETs with multiple molecular propellants, which this paper aims to accomplish. The expected performance of a low-power HET operating on molecular propellants is expected to be very low due to the drawbacks that both low-power HETs and molecular propellants suffer from individually. In this study, we investigate the performance of a low-power HET (< 500 W) called Simplified CAMILA (Co-Axial Magneto-Isolated Anode) operating on Xe, Kr, Ar, N_2, and CO_2. This is to assess the capability of operating a low-power HET on molecular propellants and explore the performance characteristics of the thruster by comparing molecular propellants with the conventional and well-studied atomic gases.

II. Experimental Setup

A. Test Article

The full CAMILA Hall thruster is a Thruster with Anode Layer (TAL) magnetically-shielded HET developed by the Technion, but in this experiment we used Simplified CAMILA, the non-magnetically-shielded cousin.

Henceforth, the thruster will just be referred to as CAMILA. Figure 1 shows a schematic of the CAMILA Hall thruster. The ionization of propellant is produced mainly in the anode cavity that is formed by two coaxial metallic cylinders, which are held at the anode potential, and an end face of the gas distributor, which is under a floating potential. In the anode cavity, the longitudinal magnetic field is applied. It is produced by outer and inner anode magnetic coils with electric currents in opposite directions, and the magnetic screens. The propellant enters the cavity through the gas distributor. It is ionized by electrons, which oscillate between the end face of the gas distributor and the exit of the cavity. At a sufficiently strong magnetic field in the cavity, it is possible to form a radial electric field, directed to the middle surface of the cavity, in spite of the radial gradient of electron pressure. This radial electric field keeps ions from colliding with the cylindrical walls of the cavity. The length of the cavity is varied to obtain a high degree of propellant ionization. After leaving the anode cavity, the ions are accelerated by a longitudinal electric field in the acceleration channel.

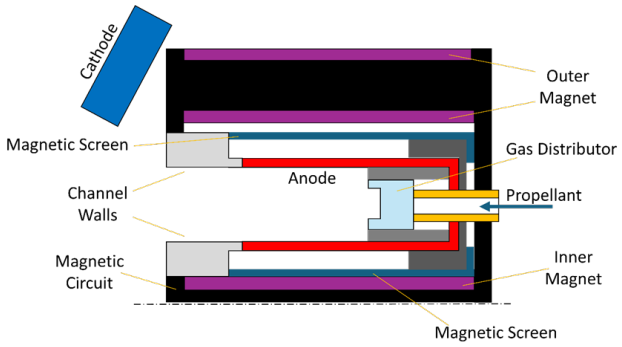

Figure 1: Schematic of the CAMILA low-power HET.[15]

The experiments were conducted using a cathode-neutralizer procured from Plasma Control LLC, Colorado, USA. Figure 2a shows a CAMILA CAD cross-section. Figure 2b shows a picture of the actual thruster with dimensional callouts. Table 3 displays key CAMILA dimensions and xenon performance metrics. A dedicated ignition block (I/B) supplies the high voltage pulse necessary to ignite the cathode, as well as the keeper holding voltage required to sustain emitter-keeper plasma after cathode discharge is set. The thruster discharge voltage is supplied by the main power supply that connects between the anode and cathode. Two power supplies feed current to the magnetic circuit; one to the outer coils and the other to the central coil. This arrangement enables small magnetic field topology adjustments during tests in the event that unexpected thruster behavior is encountered.

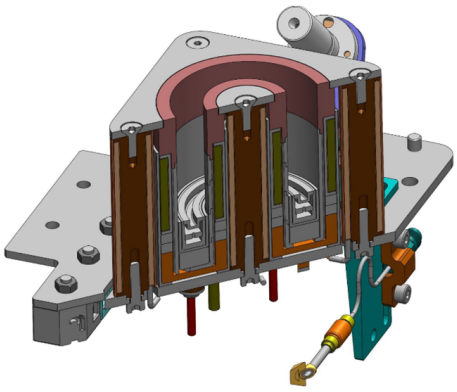

(a) CAD illustration cross-section.

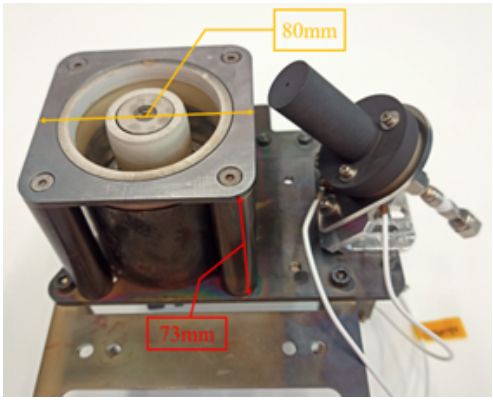

(b) Picture of CAMILA.
Thruster dimensions are marked on the picture.

Figure 2: CAMILA HT images

Table 3: CAMILA performance parameters with xenon propellant.[16]

Channel Mean Diameter	49 mm
Channel Width	12 mm
Power Range	150-300 W
Thrust Range	10-20 mN
Specific Impulse	1400-1900 s
Anode Efficiency	40-55%
Cathode mass flow rate (Xe)	1.50 sccm

B. Facilities

Performance tests were conducted at the Asher Space Research Institute (ASRI) electric propulsion laboratory at the Technion. The test facility includes a 1.22 m $\varnothing \times 2.7$ m stainless steel vacuum chamber with an inner volume of approximately 3.2 m^3. The chamber is equipped with a RUTAWAU 501/D65B/A forevacuum pump with a pumping speed of 230 L/s of air. Three Sumitomo CP-22 cryopumps are located opposite the thruster. The combined measured pumping speed achieved is approximately 9,000 L/s on xenon. The residual pressure of the vacuum chamber is lower than 9×10^{-8} Torr. During thruster operation at a total flow rate of 1.2 mg/s of xenon, chamber pressure was lower than 2×10^{-5} Torr (xenon corrected). It should be noted that this chamber pressure value is expected to affect thruster performance due to residual vacuum chamber gas ingested by the thruster. Suitable calculation of the effect on thruster performance can be found in the Appendix.

Figure 3 shows a diagram of the ASRI vacuum chamber. Pressure is measured using an Ionivac sensor (model ITR90 from Leybold) located behind the thruster. The Ionivac pressure gauge is calibrated by the manufacturer and has a declared precision of 15%. A commercial flow controller, capable of measuring flow rate from 0 to 1.96 mg/s, model M100b from MKS, controls gas flow to the thruster's gas distributor. Similarly, a flow controller controls the flow rate to the cathode, from 0 to 0.98 mg/s, and was set to either 0.15 mg/s or 0.20 mg/s (exclusively xenon) during all tests. The mass flow controllers are calibrated by the manufacturer, with a declared precision of 1% of full scale.

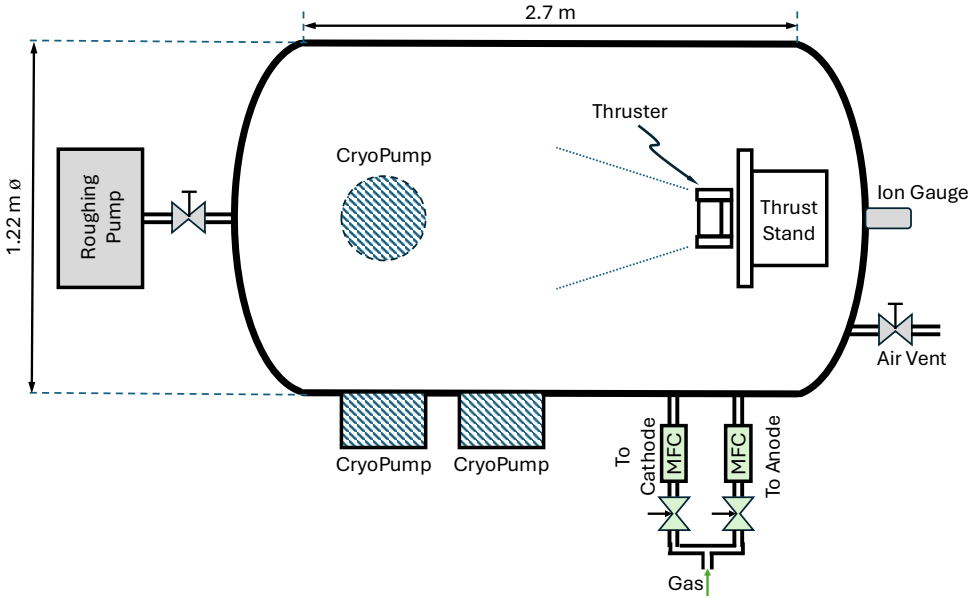

Figure 3: Schematic of the Asher Space Research Institute (ASRI) electric propulsion laboratory experimental facility.
(not to scale)

C. Diagnostics

The thrust stand used is a feedback-controlled inverted pendulum type, manufactured for ASRI by PLATAR LTD, Moscow, Russia. It is capable of thrust measurements from 1 to 200 mN. Measurement accuracies, as declared and verified by the manufacturer, are ±3.5% between 5 and 10 mN and ±3% between 10 and 20 mN. During tests, the thrust stand measurement was recorded; after the thruster was shut off, the number that the thrust stand read was recorded and subtracted from the measurement taken during operation. In this fashion, the thrust stand was "zeroed." An oscilloscope was used to measure the fluctuations in discharge current draw with a sampling frequency of 5.0×10^7 Hz for Xe, Kr, Ar, N_2, and 5.0×10^6 Hz for CO_2. However, we did not methodically take frequency measurements, so we refer to discharge frequency in a qualitative manner.

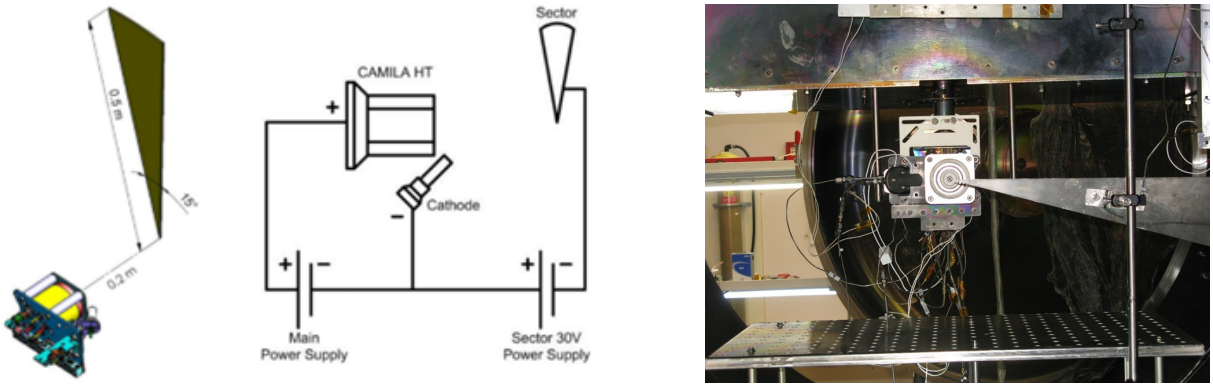

Figure 4: Diagram and picture of the angular Faraday probe.[15]

A 15° angular Faraday probe "pizza slice" was aligned with the thruster's central axis, as shown in Fig. 4, in order to measure the ion current of the exhaust plume. It is manufactured from stainless steel. The large radius of the receiver and small angle of the arc allow both the measurement of ions from exhaust plumes with large divergence angles, and prevents noticeable influence of the ion receiver on the thruster parameters. While taking measurements, the potential of the probe was biased by −30 V with respect to the cathode. At such a bias, the current in the circuit of the sector ceased to depend on the potential of biasing. The value of the full ion current is simply the value measured by the pizza slice multiplied by 24 (since $15° \times 24 = 360°$). Secondary electron emission, due to ion and electron bombardment of the probe surface, can also lead to errors in measurement. However, these effects are relatively small (less than 10%) under thruster conditions.[17] Thus, the recorded ion current is corrected by a factor of 10% estimating the influence of the receiver's ion-electron emission on the ion current measurement. This 10% is also used as the error for this diagnostic in subsequent error analysis.

D. Experimental Methods

Table 4 highlights key relevant properties of the gases examined in this study. We can see that xenon is the energetically easiest to ionize and helium the most difficult. Despite CO_2 and N_2 having lower ionization energies than argon, they have an even lower dissociation energies, which creates a power sink as energy spent dissociating and not ionizing molecular propellants is wasted energy. Only ionization events will generate meaningful amounts of thrust.[2]

Table 4: Leading gas properties for the propellants used in this study.

Gas	Mass (amu)	1st Ionization Energy (eV)	Dissociation Energy (eV)	Relative Cost ($USD/kg)	Literature
Xe	131.29	12.1	-	1200	[16]
Kr	83.798	14.0	-	500	[14]
Ar	39.948	15.8	-	5	[14]
CO_2	44.009	13.7	5.45	0.10	[10,12]
N_2	28.014	15.58	9.76	0.20	[11,14]
He	4.0026	24.6	-	50	[18]

Table 5 shows the range of input parameters over which we operated. Throughout testing we collected data for all gases operating at both constant power (400 W and 450 W), constant voltage (250 V) and varying magnetic fields, and constant voltage and power (250 V and 350 W, 400 W, 450 W). Constant power is useful because the power processing units (PPU) of spacecraft are designed to deliver a fixed amount of power to components such as the thruster.

Table 5: Range of test parameters

Propellant	Voltage Range	Anode Mass Flow Rate		Power	B Field Strength	Cathode Mass Flow Rate (Xe only)	
	V	sccm	mg/s	W	G	sccm	mg/s
Xe	75-418	12.0-22.0	1.180-2.163	76.50-450.00	117.5-211.5	1.50-2.00	0.15-0.20
Kr	100-407	15.0-29.4	0.935-1.832	170.00-450.93			
Ar	160-266	28.0-36.0	0.832-1.069	277.44-450.07	90.0-118.1		
CO_2	150-250	33.0-48.0	1.079-1.570	72.00-450.00	248.3-292.1		
N_2	180-250	55.0-75.4	1.144-1.568	211.50-451.56			

III. Results and Discussion

The thruster was successfully operated on Xe, Kr, Ar, N_2, and CO_2 at points listed above in Table 5. A helium-neon mix was attempted, but the thruster was unable to be ignited under any conditions; therefore, the He-Ne mixture was left out of this paper, less this brief section. Images of the thruster successfully operating on the five gases can be seen in Fig. 5.

Figure 5: Thruster operating on five gases: xenon, krypton, argon, CO_2, and N_2.

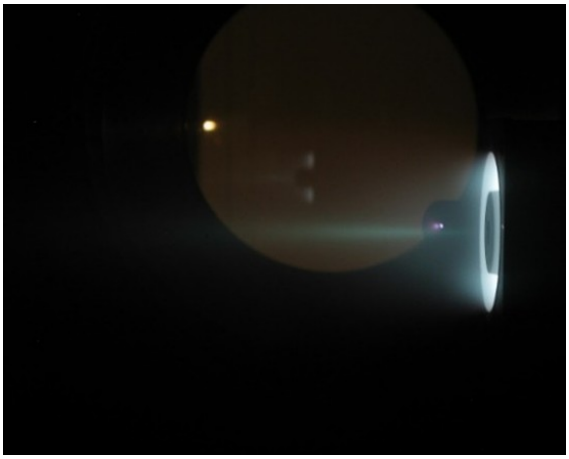

(a) Xenon (Xe)

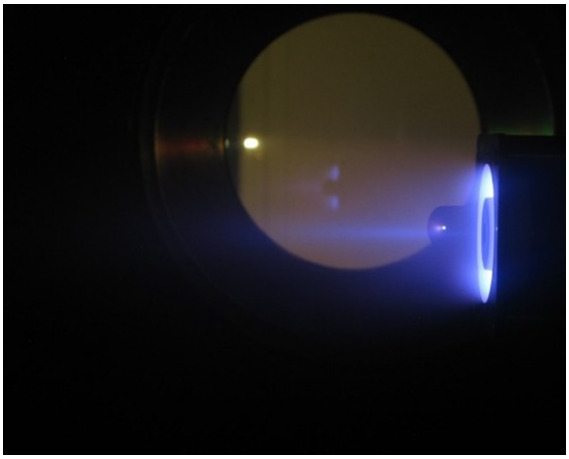

(b) Krypton (Kr)

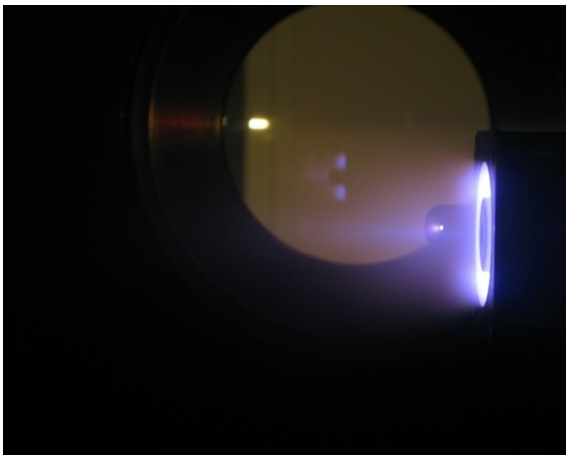

(c) Argon (Ar)

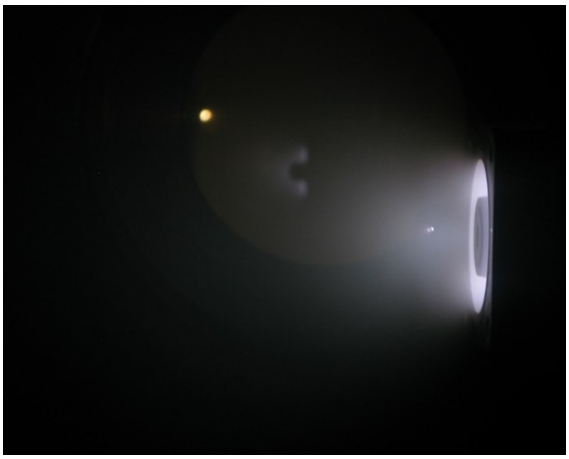

(d) Carbon Dioxide (CO_2)

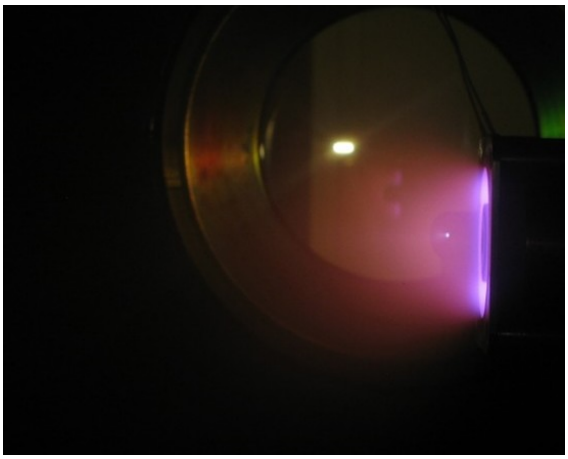

(e) Nitrogen (N_2)

Peak anode efficiencies and associated performance metrics achieved for each propellant are presented in Table 6.

Table 6: Peak efficiencies achieved.

Propellant	Voltage	Anode Mass Flow Rate		Power	Thrust	Specific Impulse	Anode Efficiency
	V_d	$\dot{m}_A$	$\dot{m}_A$	P_d	T	I_{sp}	η_A
	V	sccm	mg/s	W	mN	s	%
Xe	375.00	12.00	1.180	400.13	21.45	1853.63	48.74
Kr	346.00	19.00	1.184	449.80	18.75	1614.41	33.01
Ar	262.00	31.00	0.921	448.54	13.70	1516.82	22.72
CO_2	200.00	45.10	1.475	450.00	12.45	860.55	11.68
N_2	250.00	55.00	1.144	400.00	8.20	730.67	7.35

A. Operational Envelope

The operational envelope defines the regime—expressed as a combination of discharge voltage and mass flow rate—within which the thruster can maintain steady-state operation. The operational envelope is plotted by probing the minimum combinations of discharge voltage and mass flow rate. During testing, the thruster experienced numerous spontaneous, unplanned shutdowns, particularly when operating with light gases. Each operating point was established by selecting a specific combination of discharge voltage, mass flow rate, and magnetic field strength, while monitoring the ability of the thruster to sustain plasma discharge (henceforth referred to as stability)

We observed that the lighter the propellant gas, the more sensitive the discharge current—and consequently the discharge power—became to variations in these operational parameters, especially discharge voltage. In many instances, the thruster spontaneously shut down and had to be restarted, requiring a new, more stable combination of parameters to sustain operation.

To probe the operational boundary for each propellant, we initiated thruster ignition at known stable points and then gradually decreased either the discharge voltage, by 0.5–5.0 V, or the mass flow rate, by 0.1–2.0 sccm, at time intervals of one minute or longer.

To characterize the regions of operational stability—defined as the ability to sustain discharge for more than five minutes—we sought the operational envelope for each propellant. For each case, the thruster was ignited and brought to a specific operating point (a combination of discharge voltage and mass flow rate) at a constant magnetic field (see Table 5). The thruster was then observed for at least five minutes. If a spontaneous shutdown occurred, the mass flow rate was increased, the thruster reignited, and the process was repeated, making this mapping process very arduous and time-intensive. The objective was to determine the minimum discharge voltage for each propellant and the minimum mass flow rate for various discharge voltages.

Figure 6 shows the resulting minimum V_d and $\eta_{\dot{m}}$ operating points for all five propellants, representing the lowest combination of discharge voltage and mass flow rate that ensures continuous operation for at least five minutes. It is evident that xenon exhibits the widest operational envelope. At discharge voltages above approximately 200 V, the HET can operate at mass flow rates as low as ~ 7 sccm while maintaining continuous operation. All propellants show a downward trend at lower voltages, indicating that higher mass flow rates are required to sustain operation in this regime. This behavior is attributed to the need to maintain a minimum collision frequency to ensure sufficient ionization. A reduction in discharge voltage leads to lower electron temperatures and reduced electron drift velocities, both of which decrease collision frequency and ionization cross-section.[2,19] To compensate, plasma density must increase, which is achieved by increasing the mass flow rate.

Figure 6 also shows that lighter gases require higher mass flow rates—which correspond to a greater number of injected particles per unit time—to sustain stable thruster operation. This is due to the need for a larger number of particles to undergo ionization in order to maintain sufficient plasma density. Light gases tend to have lower ionization cross-sections, which can be compensated for by increasing the number of neutral particles introduced into the discharge channel, thereby supporting a higher electron density.[20,21]

Furthermore, the slope of the minimum operating condition curve is steeper for lighter propellants. This provides a quantitative indication of the increased sensitivity of thruster stability to changes in discharge

voltage when using light gases. For these propellants, a reduction in discharge voltage results in a more significant drop in ionization cross-sections compared to heavier gases. This is due to the higher electron temperature thresholds required for ionization, as well as additional energy losses to dissociation and excitation of vibrational and rotational modes.[22,23,24,25] From an engineering perspective, this sensitivity implies that thruster operation with light propellants is constrained to a narrower voltage range, or alternatively, requires a propulsion feed system capable of accommodating a wide range of mass flow rates.

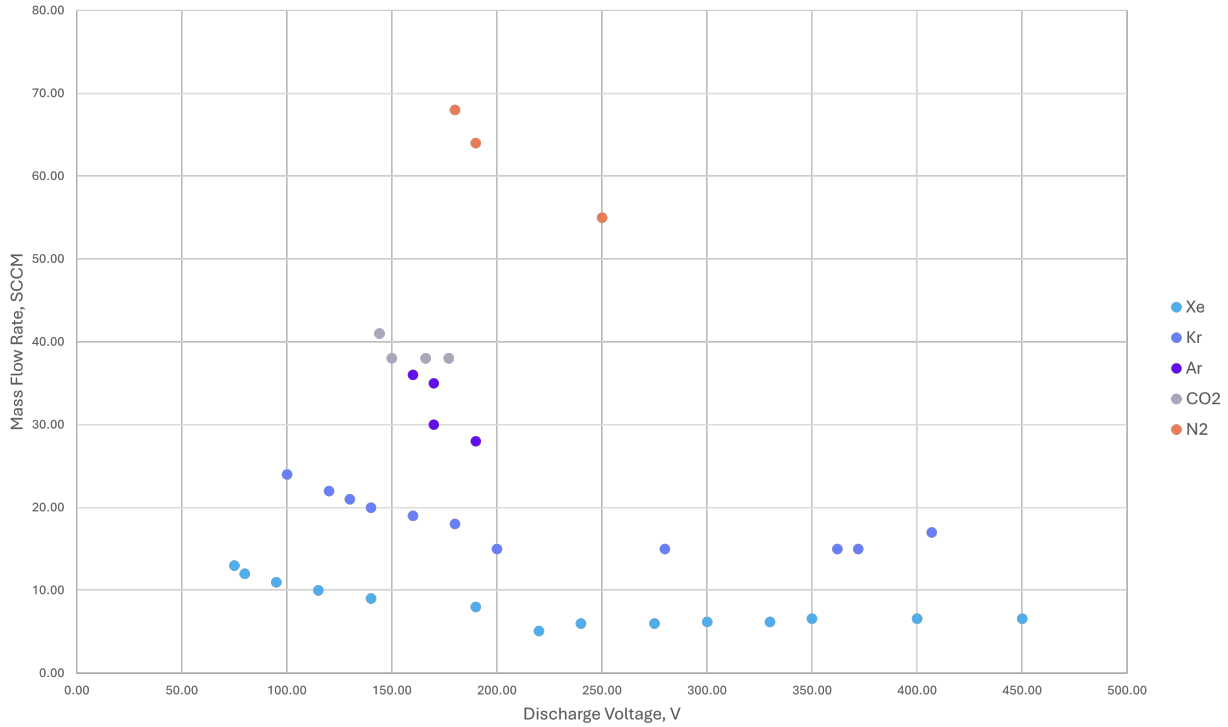

Figure 6: Operation envelope.
Minima points that allow stable thruster operation (>300s) without thruster spontaneous shutdown.

In addition to identifying operational limitations, we examined the sensitivity of discharge power to variations in operating parameters. Different combinations of discharge voltage and mass flow rate can yield the same discharge power, though with differing performance characteristics. To explore this relationship across various propellants, we superimposed the operating points of constant power on top of the operational envelope from Fig. 6. These constant power points are shown in Fig. 7. It is evident that as the propellant becomes lighter, the discharge power becomes more sensitive to changes in discharge voltage as these propellants require a higher volumetric flow rate to sustain operation. This trend aligns with the previously discussed limitations associated with light gases.

Additionally, we included non-unique, interpolated equi-power lines that span across different propellants. While an infinite number of such lines could be drawn, those shown in Fig. 7 serve to contextualize the transition regions between propellants when discharge power is held constant. These lines help illustrate how the operational regime shifts as a function of propellant type under equivalent power conditions.

The first main takeaway from Fig. 7 is that as we go to lower atomic masses, we must go to lower discharge voltages and higher mass flow rates. The converging nature of the equi-power curves provides the clearest evidence of increased sensitivity with decreasing propellant atomic mass. As the propellant becomes lighter, the operational space narrows and becomes more sensitive to variations in discharge voltage, highlighting the challenges of maintaining stable operation with low-mass gases.

For each individual gas, the equi-power lines are expected to have a $\frac{1}{x}$ relation due to the relationship explained in Eq. (1):

$$P_d = V_d I_d \propto V_d \frac{\dot{m}_A}{m}, \tag{1}$$

where P_d is discharge power, V_d is discharge voltage, I_d is discharge current, $\dot{m}_A$ is anode mass flow rate, and m is propellant neutral mass. This trend is indeed observed within each propellant data set. This formulation implies that for a given power level, the product of voltage and volumetric flow rate should remain constant across different gases, assuming similar ionization behavior. Therefore, in theory, all propellants should lie on the same equi-power curves—effectively "stacked" on top of one another—regardless of their atomic mass. However, the experimental data reveal a deviation from this idealized scaling. As we transition to lighter propellants, the equi-power lines shift upward, indicating that a higher volumetric flow rate is required to maintain the same power. This behavior is expected due to the lower ionization cross-sections of lighter gases, which necessitates injecting more particles to achieve sufficient plasma density and sustain discharge. The increased particle injection compensates for the reduced ionization cross-section and higher energy losses to dissociation and excitation modes, particularly in molecular gases.[26]

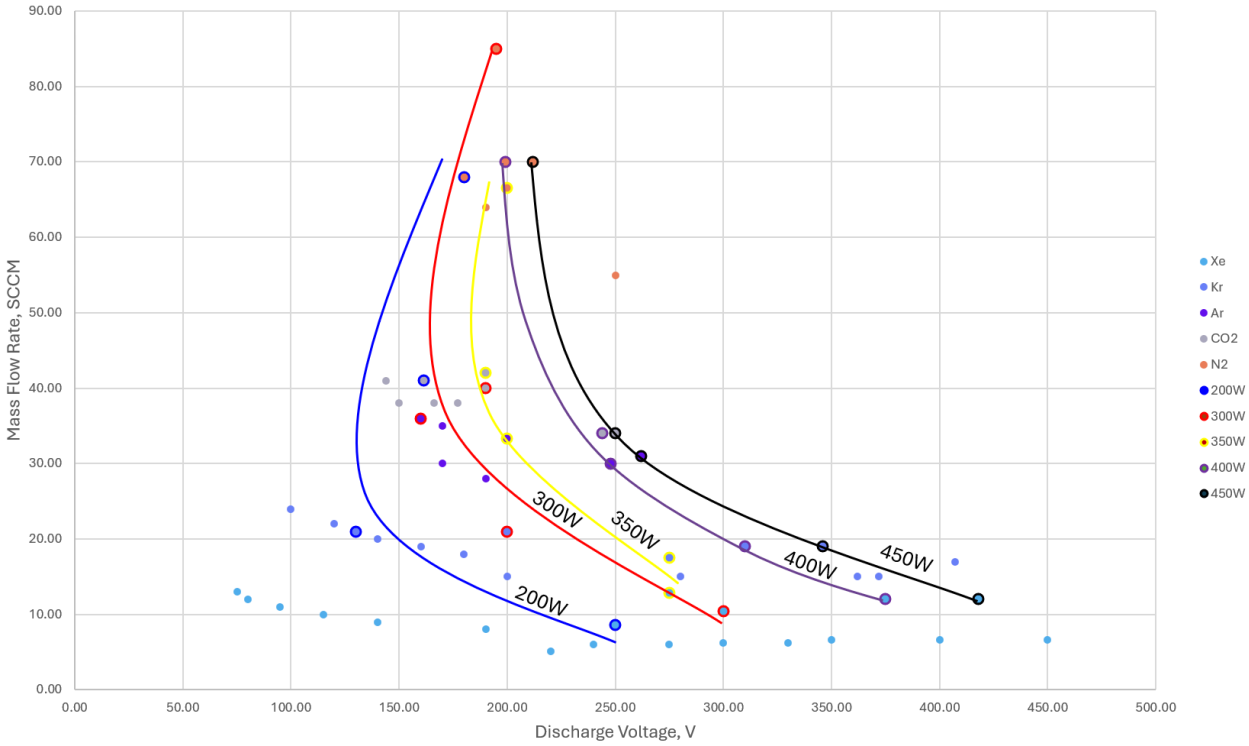

Figure 7: Operation envelope with non-unique equi-power lines.
The bullet color represents the gas type while the bullet outline color (for relevant points) represents the power level.

The unexpected observation here is that in some cases, the discharge voltage must decrease rather than increase to maintain constant power. This contradicts the theoretical scaling and suggests the presence of parasitic effects. One plausible explanation is the onset of high discharge currents—possibly due to elevated collision frequencies—when operating with lighter gases. As more particles are injected to compensate for poor ionization, the electron-neutral collision rate increases, potentially leading to enhanced electron mobility and axial current leakage.[27] To prevent exceeding the power supply limits, we reduced the discharge voltage, thereby maintaining the desired power level despite the increased current draw. This phenomenon highlights a complex interplay between discharge voltage, mass flow rate, and plasma behavior that is not fully captured by simple scaling laws. It suggests that lighter gases introduce additional loss mechanisms and nonlinearities in the discharge process, which merit further investigation. Future work should focus on characterizing these parasitic currents and exploring whether tailored magnetic field topologies could mitigate their impact and restore the expected scaling behavior. We had to increase the magnetic field strength by 48% for molecular propellants versus xenon because that was the only way to ensure operation.

When we move to lighter propellants, we must overcome ionization issues by introducing more particles or increasing the energy transferred to particles. Increasing discharge voltage V_d will increase electron

temperature T_e and therefore the ionization rate coefficient K_i, while increasing the mass flow rate $\dot{m}_A$ will increase the neutral particle number density n_0. Equation (2) demonstrates the factors that contribute to ionization:

$$\frac{\partial n_i}{\partial t} = n_e n_0 K_i(T_e), \tag{2}$$

where $\frac{\partial n_i}{\partial t}$ is the time rate of change of the ion number density, n_e is the electron number density, n_0 is the neutral particle number density, and $K_i(T_e)$ is the ionization rate coefficient as a function of electron temperature. Increasing either of these input parameters (V_d or $\dot{m}_A$) should theoretically improve our ionization ($\frac{\partial n_i}{\partial t}$), however we are forced into increasing $\dot{m}_A$ as increasing V_d introduces instabilities that prevent stable thruster operation.

The final takeaway from Fig. 7 is the "bunching" of equi-power lines observed with N_2. Nitrogen is known to be particularly challenging and unstable during HET operation,[26] often requiring high mass flow rates to maintain ignition. This limits the ability to reduce overall power consumption, making it less flexible compared to other propellants and greatly limiting the operational region, even more so than heavier CO_2. Argon and CO_2 exhibit similar operational envelope boundaries due to their comparable atomic/molecular masses. However, CO_2 introduces additional energy dissipation mechanisms verses Ar, including dissociation, as well as rotational and vibrational excitation, which influence its discharge behavior and further shift its operational envelope upwards (in terms of mass flow rate) on Figs. 6 and 7.

B. Constant Voltage and Constant Discharge Power

In order to obtain a side-by-side comparison of all propellants at the same discharge voltage and power, we were forced to constrain discharge voltage to 200 V as both molecular propellants require higher mass flow rates (and thus higher powers) to operate at higher discharge voltages. Once again, performance in key metrics, including thrust, I_{sp}, and η_A, in decreasing order, are: Xe, Kr, Ar, CO_2, and N_2. The exception to this is argon, having a 1.8% greater I_{sp} than krypton at 450 W. Notably, CO_2 provides similar thrust to Ar, but with lower I_{sp} and anode efficiency. Mass utilization efficiency $\eta_{\dot{m}}$ is defined in Eq. (3), beam or current utilization efficiency η_b is defined in Eq. (4), and overall anode efficiency η_A is defined in Eq. (5):

$$\eta_{\dot{m}} = \frac{\dot{m}_i}{\dot{m}_A}, \tag{3}$$

where $\dot{m}_i$ is ionized mass flow rate and $\dot{m}_A$ is anode (or total) mass flow rate,

$$\eta_b = \frac{I_b}{I_d}, \tag{4}$$

where I_b is beam current and I_d is discharge current, and

$$\eta_A = \frac{\dot{m}_i v_i^2}{2P_d}, \tag{5}$$

where v_i is ion exhaust velocity and P_d is discharge power. Figure 8 shows these three internal efficiencies as a function of propellant and power with error bars. Table 7 presents the numerical data.

Overall, anode efficiency is highest for xenon, followed by krypton, argon, CO_2, and N_2. Mass utilization efficiency increases as the mass flow rate and thus power increases across all propellants. We postulate that as the mass flow rate is increased, so is the corresponding number density, leading to a higher collision frequency and a higher ionization fraction. This behavior is more prominent for gases with either a high ionization potential, such as krypton, or a high number of electron energy sinks,[26] such as molecular propellants. Since these gases see a relatively low degree of ionization[26] any improvement in collision frequency will result in an increase in the mass utilization efficiency. Since ionization is very low in molecular propellants, the increase in mass utilization efficiency will also lead to an increase in the overall efficiency. We estimate that this increase in efficiency with mass flow rate can benefit the ionization up to a certain point, after which the gas is fully ionized, and any increase in plasma density contributes to reducing the Hall parameter and inducing a higher electron mobility.[27] To support this postulation, it was previously found that increasing the mass flow rate and thus discharge power past a certain point results in a decrease in $\eta_{\dot{m}}$ and thus overall η_A.[28] The assumption was made that every ionization led to a charge of +1; therefore, the $\eta_{\dot{m}} > 1$ as seen with Xe is not physical but a result of double and triple ionization events.

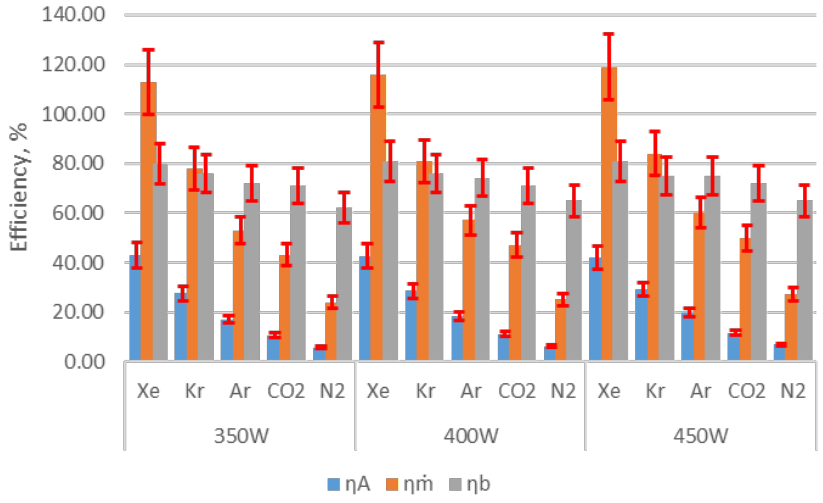

Figure 8: Thruster efficiencies for fixed voltage (250 V) and fixed power.

Table 7: Fixed voltage and power measured results.

Discharge Power	Propellant	Anode Mass Flow Rate		Cathode Mass Flow Rate (Xe)		Ratio of I_{inner}/I_{outer} Magnet Coils	Discharge Voltage	Discharge Current	Thrust	Specific Impulse	Anode Efficiency	Mass Utilization Efficiency	Current Utilization Efficiency
P_d		$\dot{m}_A$	$\dot{m}_A$	$\dot{m}_A$	$\dot{m}_A$	B_{ratio}	V_d	I_d	T	I_{sp}	η_A	$\eta_{\dot{m}}$	η_b
W		sccm	mg/s	sccm	mg/s		V	A	mN	s	%	%	%
350	Xe	17.3	1.701	1.50	0.15	2.286	200	1.750	22.60	1354.68	42.91	113	80
	Kr	23.8	1.483						16.90	1161.65	27.51	78	76
	Ar	33.3	0.989	2.00	0.20	2.000			10.85	1118.30	17.00	53	72
	CO_2	40.6	1.328			1.143			9.95	763.98	10.65	43	71
	N_2	64.4	1.340			1.139			7.25	551.72	5.61	24	62
400	Xe	19.3	1.897	1.50	0.15	2.286		2.000	25.40	1364.74	42.51	116	81
	Kr	26.1	1.626						19.30	1209.72	28.63	81	76
	Ar	36.4	1.081	2.00	0.20	2.000			12.60	1188.07	18.36	57	74
	CO_2	42.4	1.386			1.143			11.10	816.09	11.11	47	71
	N_2	70.9	1.475			1.139			8.60	594.46	6.27	25	65
450	Xe	21.1	2.074	1.50	0.15	2.286		2.250	28.00	1376.10	42.00	119	81
	Kr	28.3	1.763						21.50	1242.85	29.13	84	75
	Ar	39.2	1.164	2.00	0.20	2.000			14.45	1265.19	19.93	60	75
	CO_2	45.1	1.475			1.143			12.45	860.55	11.68	50	72
	N_2	74.2	1.543			1.139			9.70	640.67	6.77	27	65

As for the current utilization efficiency, we see for all types of propellants that the beam efficiency generally increases with mass flow rate and thus power. We can attribute this to improved ionization by increasing the collision frequency with the addition of mass flow rate, that in turn increases the ion beam current. However, unlike with mass utilization efficiency, there is very little difference between the beam efficiency of the different gases. We postulate that this is due to the following. Beam efficiency is a function of the ion beam current and the discharge current carried by the electrons. A poorly ionized propellant will result in both low beam current and low discharge current. This can result in a similar ratio regardless of the degree of ionization. Since the ionization length is larger in molecular propellants due to the dissociation region (the average ion is born further downstream than atomic propellants) and a longer ionization mean free path,[26] we can assume that a non-negligible fraction of the ion beam may result in a large divergence angle that will reduce the axial momentum, thus reduce the thrust.

To further investigate the physical processes behind the behavior of the mass utilization efficiency, we adopt Hurley's model.[29] Equation (6) presents an expression for the mass utilization efficiency that projects $\eta_{\dot{m}}$ as a function of plasma parameters:[29]

$$\eta_{\dot{m}} = 1 - exp\left(-\frac{\langle n_e \rangle \langle k_{iz}(T_e) \rangle}{v_n} \bar{L}\right), \tag{6}$$

where n_e is electron number density, $k_{iz}(T_e)$ is the total ionization rate coefficient averaged over a Maxwellian e^- population with T_e, v_n is the thermal velocity, $\bar{L}$ is the characteristic length of the thruster, and $\langle\rangle$ denotes average quantities. Hurley then estimates the mean free path for ionization (λ) as a function of HET operational parameters in Eq. (7), cited in Hurley's paper as Equation 9, and finally arrives at Eq. (8), cited in Hurley's paper as Equation 10, which is what we will use to apply this model to molecular propellants:

$$\lambda_i = \sqrt{\frac{T_n k_b}{m_i}} * \frac{(V_d - V_{CC})\alpha q}{L_{acc} B (1-\eta_b)\langle k_{iz}(T_e)\rangle j_D}, \tag{7}$$

$$\eta_{\dot{m}} = 1 - exp\left(\frac{\bar{L}}{\lambda_i}\right), \tag{8}$$

where i is the subscript for any given propellant, T_n is neutral gas temperature , m is propellant atomic/molecular mass, k_b is the Boltzmann constant, V_d is discharge voltage, V_{CC} is the cathode coupling voltage, α is the inverse of the Hall parameter, q is the elementary charge, L_{acc} is the acceleration region length, B is the magnitude of the magnetic field, $k_{iz}(T_e)$ is the total ionization rate coefficient averaged over a Maxwellian e^- population with T_e, and j_D is the discharge current density (discharge current over discharge channel area at the exit plane). V_{CC} was estimated at a constant 20 V, T_n at 400 K, L_{acc} as 10 mm,[30] and $\bar{L}$ as 20 mm. $|B|$ was calculated using Finite Element Method Magnetics (FEMM) software at the exit plane in the center of the discharge channel. Hurley states that α should fall in between 0.01 and 0.001.[29] The calibration of α was done for Kr with T_e as 25 eV, where we approximate T_e as $0.1V_d$,[31] to exactly equal the actual measured $\eta_{\dot{m}}$ value for Kr at 400 W discharge power; α was calibrated to Kr and not Xe because of the aforementioned empirical value for Xe of $\eta_{\dot{m}} > 1$. The calibrated α is consistent with the range of values Hurley cites in his paper of $\alpha \in (0.001, 0.01)$. Figure 9 shows mass utilization efficiency as a function of propellant with α constant across all propellants. It should be noted that though we held α constant for the purposes of this model, we expect the Hall parameter to decrease for molecular propellants. This is due to axial leakage currents caused by increased electron-neutral collisions that come with the high mass flow rates required for stable molecular propellant operation.

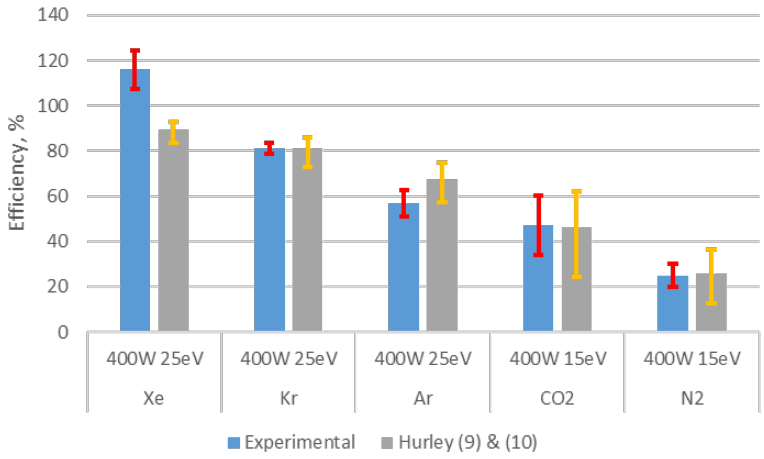

Figure 9: Real vs Hurley's model $\eta_{\dot{m}}$.

CO_2 and N_2 are plotted assuming a T_e of 15 eV since molecular propellants have been shown to have lower electron temperatures.[26] Brabston posits the following relationship for nitrogen T_e in Eq. (9):[26]

$$T_{e,N_2} \approx 0.1 V_d \sqrt{\frac{m_{N_2}}{m_{Xe}}}, \tag{9}$$

where T_{e,N_2} is N_2 electron temperature, V_d is discharge voltage, m_{N_2} is N_2 neutral mass, and m_{Xe} is xenon neutral mass. This would yield a T_{e,N_2} of 11.5 eV, falling in the error margin of our assumption of 15 eV. The error bars for Hurley's model are plotted using T_e = (20 eV, 30 eV) for the three inert propellants,

and T_e = (10 eV, 20 eV) for the two molecular propellants. For all gases operating in this power regime, assuming a higher T_e yields a higher $\eta_{\dot{m}}$.

Equations (7) and (8) are extremely sensitive due to the exponential terms, causing a lot of noise from even small deviations from true values. Thus, this analysis serves as a qualitative measure of how Hurley's model holds up for molecular propellants, rather than a quantitative analysis looking to appraise the exact deviation from the model.

C. Fixed Voltage Varying Magnetic Field

Xenon had the highest mass and current utilization efficiencies ($\eta_{\dot{m}}$ and η_b) as well as the highest overall anode efficiency (η_A), followed by krypton, as was expected. We largely omitted argon from this experiment due to its unmapped efficiency peak. The two molecular propellants had the worst overall efficiencies, with CO_2 performing better than N_2. CO_2 and Ar have relatively similar $\eta_{\dot{m}}$ and η_b values, yet Ar has a significantly higher η_A, indicating that Ar has a better voltage utilization efficiency, η_V, multiplied by the beam divergence efficiency, γ, than CO_2. Specific impulse, I_{sp}, behaved as expected, with Xe having the highest I_{sp} followed by Kr, Ar, CO_2, and N_2.

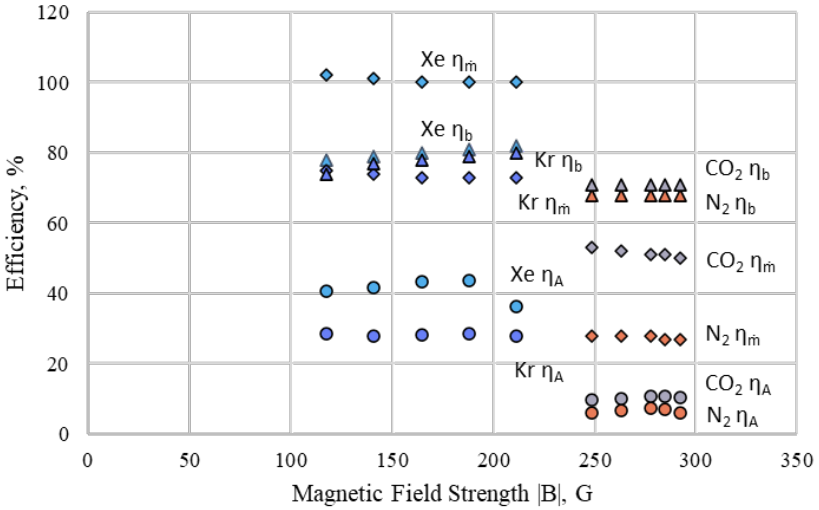

Figure 10: Internal efficiencies as a function of B field strength.

The cathode-to-ground voltage (V_{CG}) changed less for the various magnetic field configurations of the molecular propellants, approximately 1 V for CO_2 and N_2, than it did for the inert propellants, approximately 2.5 V for Xe, Kr, and Ar. The current ratios were held constant for each propellant, so the magnetic topology was fixed, as seen in Fig. 11; only its magnitude was adjusted.

Figure 11: B field configuration for four gases: Xe, Kr, CO_2, and N_2.

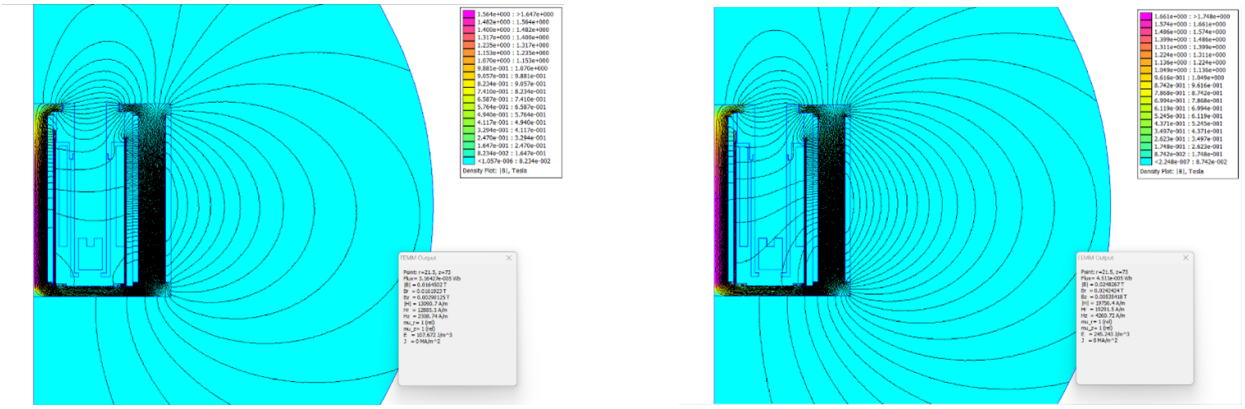

(a) $B_{ratio} = 2.29$ $[Xe,\ Kr]$ **(b)** $B_{ratio} = 1.13$ $[CO_2,\ N_2]$

For all propellants, both ion beam current and discharge current were observed to decrease with increasing magnetic field strength, as seen in Fig. 12. This trend is attributed to enhanced electron confinement and reduced cross-field electron mobility.[32] Stronger confinement also reduces electron drift velocity and may promote the formation of multiply-charged ions, particularly for xenon and krypton.[33] In the case of lighter propellants, the increased magnetic field can reduce the ion cyclotron radius to values comparable to the characteristic length of the thruster. Assuming the ion velocity perpendicular to the magnetic field is $v_i = \frac{T}{\dot{m}_A}$, the cyclotron radii for singly ionized CO_2 and N_2 are approximately 16.5 cm and 8 cm, respectively, while the radius for singly ionized atomic nitrogen is about 4 cm. These values approach the characteristic dimensions of the HET used in this study, potentially leading to ion trajectory divergence.

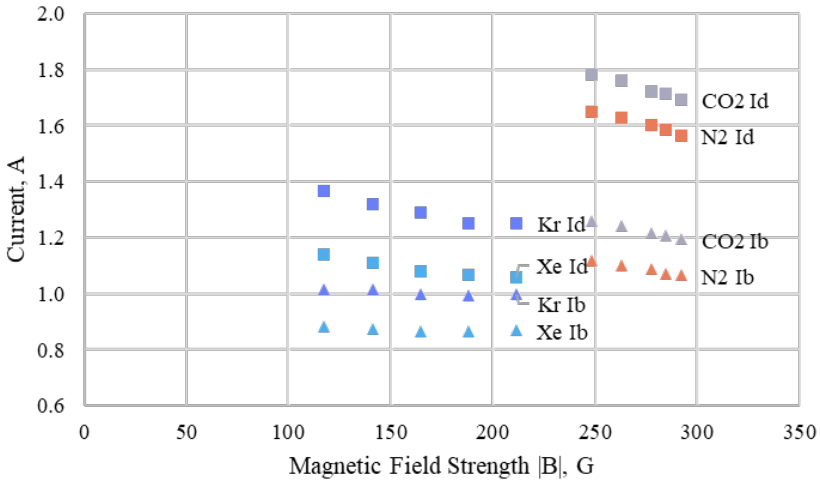

Figure 12: Discharge and beam current vs B field strength.

As the ion beam current decreases at constant anode mass flow rate, mass utilization efficiency correspondingly declines for all four gases. However, the reduction in discharge current due to stronger electron confinement is more pronounced than the reduction in ion beam current as seen in Fig. 12, resulting in an increase in beam current efficiency with increasing magnetic field strength beyond the optimal point.

The combined effect of these trends is a characteristic rise-and-fall behavior in overall efficiency for all propellants examined in this phase of the study. In summary, increasing the magnetic field beyond the optimal point initially enhances efficiency by reducing discharge current and power consumption, while maintaining sufficient—albeit slightly reduced—thrust. However, further increases in magnetic field strength eventually

led to a significant drop in ion beam current, reversing the efficiency gains and resulting in a decline in anode efficiency.

IV. Conclusion

This study provides an early performance comparison of a low-power HET operating on multiple atomic and multiple molecular propellants under matched conditions. The key finding is that while molecular propellants such as CO_2 and N_2 can sustain stable operation in a low-power HET, they do so only within significantly narrower operational envelopes and at the cost of reduced performance. Specifically, molecular gases required approximately 1.48× stronger magnetic fields and substantially higher mass flow rates than inert gases to maintain ignition and discharge stability at equal power levels. These requirements stem from lower ionization efficiencies and additional energy sinks such as dissociation and vibrational excitation, which are unique to molecular species.

The operational envelope mapping revealed that lighter gases exhibit steeper stability boundaries, indicating greater sensitivity to discharge voltage. Notably, nitrogen demonstrated the narrowest operational envelope and the lowest anode efficiency, while CO_2, though still under-performing atomic gases, showed relatively better stability and efficiency. Equi-power mapping further revealed that lighter gases deviate from the expected first-order scaling laws, requiring higher particle injection rates and, counterintuitively, lower discharge voltages to maintain constant power—likely due to axial leakage current and elevated electron-neutral collision rates.

Internal efficiencies analysis showed that anode, mass utilization, and current utilization efficiencies generally improved with increasing power across all propellants. Hurley's model for mass utilization efficiency was found to qualitatively predict trends across all gases, including molecular ones, when adjusted for lower electron temperatures.

Finally, increasing magnetic field strength initially improved performance by enhancing electron confinement but eventually reduced ion beam current—especially in molecular gases—we postulate due to increased ion trajectory divergence, highlighting an optimization problem to be considered in the operation of molecular propellants.

Appendix

A. Corrections and Error Analysis

1. *Anode Efficiency* η_A

The overall anode efficiency error bars were calculated using Eq. (10):

$$\frac{\partial \eta_A}{\eta_A} = 2\frac{\partial T}{T} + \frac{\partial \dot{m}_A}{\dot{m}_A} + \frac{\partial I_d}{I_d} + \frac{\partial V_d}{V_d}, \tag{10}$$

where η_A is anode efficiency, T is thrust, $\dot{m}_A$ is anode mass flow rate, I_d is discharge current, and V_d is discharge voltage.

2. *Mass Utilization Efficiency* $\eta_{\dot{m}}$

Mass utilization efficiency error bars were calculated using Eq. (11):

$$\frac{\partial \eta_{\dot{m}}}{\eta_{\dot{m}}} \approx \sqrt{\left(\frac{\partial \dot{m}_A}{\dot{m}_A}\right)^2 + \langle\left(\frac{\partial \Omega_{ij}}{\Omega_{ij}}\right)^2\rangle_m + \left(\frac{\partial I_b}{I_b}\right)^2}, \tag{11}$$

where Ω_{ij} is the species fraction and I_b is the beam current. Because we did not have access to an ExB probe for this experiment, we assumed $\frac{\partial \Omega_{ij}}{\Omega_{ij}} = 0$, that is, the propellant is fully and singly ionized, and the charge efficiency value is 100%. In the discussion section, we address the validity of this assumption, specifically for the molecular gases used in this test.

3. Current Utilization Efficiency η_b

Current utilization efficiency error bars were calculated using Eq. (12):

$$\frac{\partial \eta_{\dot{m}}}{\eta_{\dot{m}}} \approx \sqrt{\left(\frac{\partial I_b}{I_b}\right)^2 + \left(\frac{\partial I_d}{I_d}\right)^2}. \tag{12}$$

4. Thrust Correction T_C Using a Neutral Ingestion Model

A neutral ingestion model was used to correct recorded thrusts due to background pressure. Equation (13) demonstrates how the entrained mass flow rate was calculated:[34]

$$\dot{m}_{en} = \Phi m A_{ch} = \frac{\sqrt{m} * A_{ch} * P}{\sqrt{2 * \pi * k * T_n}}, \tag{13}$$

where $\dot{m}_{en}$ is entrained mass flow rate, Φ is particle flux, m is propellant's neutral mass, A_{ch} is discharge channel area, P is background pressure, k is the Boltzmann constant, and T_n is neutral gas temperature. Equation (14) demonstrates how corrected thrust was calculated using $\dot{m}_{en}$:[34]

$$T_C = \frac{\dot{m}_A}{\dot{m}_A + \dot{m}_{en}} T, \tag{14}$$

where T_C is corrected thrust.

B. Ignition Procedures

The ignition procedures for each propellant were tailored to ensure stable thruster operation under the constraints of the CAMILA HET and the laboratory power supply limitations. Below is a summary of the prestart conditions and ignition behavior for each gas tested.

1. Xe

Xenon ignition followed the standard procedure. Prestart conditions included a discharge power supply limit of 250 V / 1.50 A, with inner and outer magnetic coils set to 0.20 A each. The hollow cathode keeper was limited to 685 V / 0.40 A. The anode mass flow rate was set to 12.0 sccm (1.180 mg/s), and the cathode mass flow rate to 1.50 sccm.

2. Kr

Krypton ignition mirrored the procedure used for xenon. Identical prestart conditions were applied: 250 V / 1.50 A discharge limit, 0.20 A on both magnetic coils, and 685 V / 0.40 A limitation on the cathode keeper. The optimal anode mass flow rate was determined to be 19.0 sccm (1.184 mg/s), with a cathode mass flow rate of 1.50 sccm. This configuration yielded stable operation.

3. Ar

Ignition of the thruster using argon required a significant deviation from the standard procedure due to argon's high ionization energy and low atomic mass. Initial prestart conditions were set to a discharge power supply limit of 250 V / 1.80 A, with both inner and outer magnetic coils set to 0.10 A, and the hollow cathode keeper held at 685 V / 0.40 A. The anode mass flow rate was initially set to 39.7 sccm ($\sim$ 1.180 mg/s) but had to be reduced to 28.0 sccm (0.832 mg/s) to operate at a discharge voltage of 250 V, and the cathode mass flow rate was increased to 2.00 sccm to ensure stable cathode operation. At this high anode mass flow rate, the power supply operated in current-limited mode (1.80 A), and the discharge voltage remained low ($\sim$ 100 V $\pm$20 V). Attempts to transition to voltage-limited mode by increasing the magnetic field strength were unsuccessful; increasing the coil currents to $\sim$ 2.00 A in either coil resulted in thruster shutdown. To achieve stable operation at 250 V, the anode flow rate was gradually reduced to 28.0 sccm (0.832 mg/s), which enabled the transition to voltage-limited mode and reduced the discharge current. However, the magnetic coil currents remained constrained: stable operation was only possible up to 1.10 A in the outer coils and 1.78 A in the inner coil. Exceeding these values consistently led to thruster shutdowns. These limitations defined the upper bounds of magnetic field strength for argon operation in this configuration.

4. CO_2

CO_2 ignition required a lower discharge voltage and higher current limit compared to inert gases. Prestart conditions included a discharge power supply limit of 200 V / 2.00 A, magnetic coils set to 0.10 A, and the cathode keeper at 685 V / 0.40 A. The anode flow rate was initially set to 45.0 sccm ($\sim$ 1.472 mg/s), with the cathode flow rate increased to 2.00 sccm to stabilize cathode operation. Ignition was only successful at this high flow rate and low voltage. Once ignited, the magnetic coil currents were gradually increased to values exceeding 3.00 A, while the anode mass flow rate was reduced in 2 sccm increments every 30 seconds to a nominal operating point of 33.0 sccm. This gradual reduction allowed the discharge voltage to be increased to 250 V without exceeding the current limit. During initial operation, significant discharge current fluctuations ($\pm$0.25-0.30 A) were observed. These were attributed to pressure oscillations in the gas feed line. The issue was resolved by increasing the volume of the feed line—specifically, by extending the line from the gas cylinder to the low-pressure regulator by approximately 10 meters. Notably, visible erosion was observed on the thruster after extended CO_2 operation, a phenomenon not seen with other gases. This is likely due to oxygen-wall interactions resulting from CO_2 dissociation. When operating the thruster on CO_2 during the fixed voltage varying magnetic field experiment, the power supply fans could audibly be heard to ramp up or down with a period of several seconds; this in-lab experience contradicts obtained oscilloscope data that reported lower discharge current fluctuations for CO_2 versus other gases.

5. N_2

N_2 ignition was initiated with a discharge power supply limit of 275 V / 2.00 A, which stabilized at 200 V post-ignition. Magnetic coils were initially set to 0.10 A, and the cathode keeper to 685 V / 0.40 A. The anode mass flow rate was set to 70.0 sccm ($\sim$ 1.456 mg/s), and the cathode mass flow rate to 2.00 sccm to ensure more stable cathode operation. As the magnetic field was increased (¿3.00 A), the anode flow rate was gradually reduced to 55.0 sccm in the same fashion as CO_2 to enable stable operation at 250 V. Instability zones were observed at intermediate coil currents (outer: 1.20–1.50 A; inner: 1.00–1.20 A), requiring careful tuning to avoid spontaneous shutdowns.

6. He

Despite multiple attempts, the thruster could not be ignited using helium under any tested conditions.

Acknowledgments

This project was facilitated by the Birthright Israel Onward program. The authors also want to thank the Asher Space Research Institute for their hospitality while hosting the experiment.

References

[1]D. Lev, R.M. Myers, K.M. Lemmer, J. Kolbeck, H. Koizumi, and K. Polzin. The technological and commercial expansion of electric propulsion. *Acta Astronautica*, 159:213–227,, 2019.

[2]D.M. Goebel and I. Katz. Fundamentals of electric propulsion: Ion and hall thrusters. *JPL Space Science and Technology Series*, 2008.

[3]J.H. Saleh, F. Geng, M. Ku, and M.L.R. Walker. Electric propulsion reliability: Statistical analysis of on-orbit anomalies and comparative analysis of electric versus chemical propulsion failure rates. *Acta Astronautica*, 139:141–156,, 2017.

[4]S. Mazouffre. Electric propulsion for satellites and spacecraft: established technologies and novel approaches. *Plasma Sources Science and Technology*, 25(3), 2016.

[5]J.S. Snyder, D.M. Goebel, V. Chaplin, A.Lopez Ortega, and I.G. Mikellides. Electric propulsion for the psyche mission. In *36th International Electric Propulsion Conference*, Vienna, Austria, 2019.

[6]J.C. McDowell. The low earth orbit satellite population and impacts of the spacex starlink constellation. *The Astrophysical Journal Letters*, 892(2), 2020.

[7]D. Lev, R. Eytan, G. Alon, A. Warshavsky, L. Appel, A. Kapulkin, and M. Rubanovych. The development of cam200 - low power hall thruster. *Transactions of the Japan Society for Aeronautical and Space Sciences*, 14(30):217–223,, 2016.

[8]O. Hamo. A combined approach for experimental and numerical characterization of low power hall thrusters, 2024.

[9]V.-G. Tirila, A. Demairé, and C.N. Ryan. Review of alternative propellants in hall thrusters. *Acta Astronautica*, 212:284–306,, 2023.

[10]S. Tsuchikawa, S. Nishida, S. Tokuda, K. Takeuchi, and M. Matsui. Performance evaluation of a low power hall thruster with carbon dioxide propellant. *Acta Astronautica*, 2024.

[11]G. Cifali, T. Misuri, P. Rossetti, M. Andrenucci, D. Valentian, and D. Feili. Preliminary characterization test of het and rit with nitrogen and oxygen. In *47th AIAA/ASME/SAE/ASEE Joint Propulsion Conference & Exhibit*, San Diego, California, 2011.

[12]K. Hohman. *Atmospheric Breathing Electric Thruster for Planetary Exploration.* Busek Space Propulsion, Natick, MA, 2012.

[13]K. Shirasu, H. Kuwabara, M. Matsuura, H. Koizumi, Y. Nakagawa, H. Watanabe, H. Sekine, and K. Komurasaki. Demonstration and experimental characteristics of a water-vapor hall thruster. *Journal of Electric Propulsion*, 2, 2023.

[14]T.F. Munro-O'Brien and C.N. Ryan. Performance of a low power hall effect thruster with several gaseous propellants. *Acta Astronautica*, 206:257–273,, 2023.

[15]M. Rubanovich, V. Balabanov, A. Kapulkin, and E. Behar. Experimental investigations of component determining camila hall thruster performance. In *33rd International Electric Propulsion Conference*, Washington DC, USA, 2013.

[16]A. Kapulkin, V. Balabanov, M. Rubanovych, and E. Behar. Camila hall thruster: New results. In *32nd International Electric Propulsion Conference*, Wiesbaden, Germany, 2011.

[17]I. Kronhaus, A. Kapulkin, V. Balabanov, M. Rubanovich, M. Guelman, and B. Natan. Investigation of physical processes in camila hall thruster using electrical probes. *Journal of Physics D: Applied Physics*, 2012.

[18]S. Chandrasekhar and G. Herzberg. Energies of the ground states of he, li+, and o6+. *Physical Review*, 98(4):1050–1054,, 1955.

[19]Y. Raitses, A. Smirnov, Staack, and N.J. Fisch. The dependence of the electron temperature on the discharge voltage for different hall thruster configurations. In *International Electric Propulsion Conference*, Princeton, NJ, 2005.

[20]R.A. Dressler, Y.-H. Chiu, and D.J. Levandier. Propellant alternatives for ion and hall effect thrusters. In *AIAA 38th Aerospace Sciences Meeting and Exhibit*, Reno, NV, 2000.

[21]T.D. Smith, H. Kamhawi, T. Hickman, T. Haag, J. Dankanich, K. Polzin, L. Byrne, and J. Szabo. *Overview of NASA Iodine Hall Thruster Propulsion System Development.* NASA Glenn Research Center, Cleveland, OH, 2016.

[22]P. Cosby. Electron-impact dissociation of nitrogen. *The Journal of Chemical Physics*, 98(12):9544–9553,, 1993.

[23]Y. Itikawa. Cross sections for electron collisions with nitrogen molecules. *Journal of Physical and Chemical Reference Data*, 35(1):31–53,, 2006.

[24]E. Brook, M.F.A. Harrison, and A.C.H. Smith. Measurements of the electron impact ionisation cross sections of he. *Journal of Physics B: Atomic and Molecular Physics*, 11(17), 1978.

[25]X. Wang, Y. Zhang, D. Lu, G.C. Lu, B. Wei, B.H. Zhang, Y.J. Tang, R. Hutton, and Y. Zou. Fragmentation of co22+ in collisions with low-energy electrons. *Physical Review A*, 90(6), 2014.

[26]W.P. Brabston, L.A. Marino, D. Lev, and M.L.R. Walker. Hall thruster performance and efficiency analysis of a molecular propellant. *Journal of Propulsion and Power*, 2025.

[27]B. Jorns, A.Lopez Ortega, and I.G. Mikellides. First-principles modelling of the iat-driven anomalous resistivity in hollow cathode discharges i: Theory. In *52nd AIAA/SAE/ASEE Joint Propulsion Conference*, Salt Lake City, 2016.

[28]D. Lev, D.Katz Franco, B. Auslender, and O. Epstein. Extension of the operation envelope of the r-200 low. In *IEPC*. Boston, MA, 2022.

[29]W.J. Hurley and B.A. Jorns. Mass utilization scaling with propellant type on a magnetically shielded hall thruster. In *IEPC*. Toulouse, France, 2024.

[30]S.E. Cusson, E.T. Dale, B.A. Jorns, and A.D. Gallimore. Acceleration region dynamics in a magnetically shielded hall thruster. *Physics of Plasmas*, 26(2), 2019.

[31]J.M. Haas. *Low-Perturbation Interrogation of the Internal and NearField Plasma Structure of a Hall Thruster Using a High-Speed Probe.* Ph.d. dissertation,, Aerospace Engineering, University of Michigan, Ann Arbor, MI, 2001.

[32]M.J. Sekerak, B.W. Longmier, A.D. Gallimore, W. Huang, H. Kamhawi, R.R. Hofer, B.A. Jorns, and J.E. Polk. Mode transitions in magnetically shielded hall effect thrusters. In *50th AIAA/ASME/SAE/ASEE Joint Propulsion Conference*, Cleveland, OH, 2014.

[33]I. Katz, R.R. Hofer, and D.M. Goebel. Ion current in hall thrusters. *IEEE Transactions on Plasma Science*, 36(5):2015–2024, 2008.

[34]T. Randolph, V. Kim, H. Kaufman, K. Kozubsky, and M. Day. Facility effects on stationary plasma thruster testing. In *23rd International Electric Propulsion Conference*, Seattle, WA, 1993.